Behavior of light-gauge steel beams filled with recycled concrete

R. El-Nimri*ᵃ, M.S. Abdel-Jaberᵃ, Y.M. Hunaitiᵃ, M. Abdel-Jaberᵇ
ᵃ *The University of Jordan, Amman, Jordan*
ᵇ *AlHussein Technical University, Amman, Jordan*
* E-mail: rola.elnimri@gmail.com

Abstract. This paper presents an experimental and a numerical investigation of light-gauge steel box sections filled with concrete made with a combination of natural aggregate (NA), recycled concrete aggregate (RCA), and recycled asphalt pavement (RAP). A total of 47 specimens, including 30 composite beams, 15 plain concrete beams, and 2 bare steel beams were tested. The main variables in the tests were the steel thickness (2 and 2.4 mm), the coarse aggregate type and replacement ratios. NA was replaced by RCA and RAP with replacement levels of 20 %, 40 %, 60 %, 80 %, and 100 % by the total weight of NA. In addition, RCA and RAP were incorporated in the same mixes with four replacement levels of (20 % RCA and 80 % RAP); (40 % RCA and 60 % RAP); (60 % RCA and 40 % RAP); and finally, with (80 % RCA and 20 % RAP). The experimental capacities were compared to the theoretical prediction of EC4, AISC-LRFD, AIJ, and the Rigid Plastic Theory (RPT). Moreover, a finite element analysis (FEA) was performed using ABAQUS software. The experimental results showed that the ultimate capacity of composite beams decreased with the increase of RCA and RAP percentage. However, both RCA and RAP enhanced the capacity of plain concrete beams. Current code provisions predicted lower capacities than the experimental values, and the FEA results showed reasonable agreement with the test results.

1. Introduction

Introducing recycled aggregate (RA) in construction is a sustainable move in the construction industry. It prevents the consumption of current natural resources and reduces the continuous storage of waste in landfills. Recycled Concrete Aggregate (RCA) and Recycled Asphalt Pavement (RAP) are potential materials to replace natural aggregate (NA) in concrete mixes. RCA is obtained by crushing, washing, and grading concrete elements obtained from the demolition of old concrete structures while RAP is the aggregate from the base course layer obtained from roadways demolition or to gain access to buried utilities. RAP is usually reused in excavations or base layers. However, new insights are developed to use RAP in concrete mixes. When RAP is crushed and sieved, a good-quality well-graded aggregate coated with an asphalt binder layer is obtained. Several researches studied the mechanical and physical properties of concrete made with RCA [1–4]. The major conclusions are that RCA was found to compare favorably with NA but with lower strength, larger absorption, and weaker durability, nevertheless, the trend in their development was the same. Recently, other studies were conducted to investigate the effect of using RCA on the compressive, flexural and shear behavior of reinforced concrete beams [5–8]. Results proved that RCA had a small effect on the flexural and shear strength of the beams, while the progression of nonlinear behavior until failure is similar to beams with NA. It was also noted that whenever the amount of RCA increases, the initial stiffness decreases while the ultimate flexural deflections increase. Other research projects were conducted to study the effect of using RAP in concrete mixes [4], [9–11]. The major conclusions are that for low to middle strength concrete, RAP was also found to compare favorably with NA, however, the mechanical and elastic characteristics of concrete mix decrease with the increase of RAP content. This reduction in the properties of recycled aggregate concrete (RAC) needs to be minimized when it is deployed in new construction.

The composite action in concrete filled into steel tubes and the confinement of concrete infill, enhances the performance and capacity of hollow structural steel (HSS) by all sorts of applications. This could be verified due to the section transformation to be more rigid and resists more buckling [12–15]. In addition, filling hollow

steel beams provides several advantages, such as high ultimate moment of resistance, high construction speed without the need to any formwork or skilled workers, and small cross sections are needed to sustain a given load when compared to conventional reinforced beams. The major advantage of the composite action is to force the concrete infill and the steel tube to act as one unit, this interaction shifts the neutral axis upward leaving the concrete and steel above the neutral axis under compression and forces almost all the steel under the neutral axis to carry the tension force. Several research projects were conducted on composite beams made from HSS filled with mortar [13], normal concrete [14], foam, and lightweight concrete [12]. Results of previous studies showed that the bending capacity and ductility of filled and half-filled girders were higher than empty steel girders and the concrete filling enhanced the moment carrying capacity of steel hollow sections.

Because of the confinement provided by the steel tube, concrete infill is not exposed to prevailing conditions, this will enhance both the properties and behavior of the filled concrete. This characteristic if used with RAC will help to compensate the reduction of its mechanical properties. Yang and Han [16] studied the compressive and flexural behavior of recycled aggregate concrete filled steel tubes (RACFST) under short-term loadings. They stated that the behavior of RACFST is similar to the corresponding HSS columns and beams filled with normal concrete but with small reduction in capacity. It is thus expected that the RAC can be used in concrete-filled steel structures in future constructions as a replacement for hot-rolled steel or reinforced concrete structures in small to medium sized buildings. However, there is a lack of information on the behavior of light-gauge steel sections filled with RAC which indicates the need for further investigations.

Based on this literature review, this paper will investigate the flexural behavior of light-gauge steel filled with normal and recycled concrete. 15 concrete mixes divided into three groups will be considered. The first group will include five mixes with RCA at replacement levels of 20 %, 40 %, 60 %, 80 %, and 100 %. The second group will include five mixes with RAP at replacement levels of 20 %, 40 %, 60 %, 80 %, and 100 %. The third group will combine RCA and RAP together with the following percentages (1) 20 % RCA and 80 % RAP; (2) 40 % RCA and 60 % RAP; (3) 60 % RCA and 40 % RAP, and (4) 80 % RCA and 20 % RAP. One composite beam from each steel thickness and one plain concrete beam will be cast from each concrete batch, in addition, two bare steel beams will be tested as well. All beams will be tested under two-point loading. Ultimate capacities and deflections will be recorded and compared to a control specimen made with NA only. Experimental results will be compared to the theoretical prediction of EC4, AISC-LRFD, AIJ, and the Rigid Plastic Theory (RPT). Moreover, a simulation model using ABAQUS software will be made, and a finite element analysis (FEA) will be conducted.

2. Methods

2.1. Materials

2.1.1. Cement

Portland – Pozzolana Cement was used in all concrete mixes.

2.1.2. Aggregates

Fine aggregates used in this research are silica sand. While the coarse aggregates used are mainly three types: NA, RCA, and RAP. The RCA was obtained by hand crushing concrete cubes from different locations without knowing their compressive strength. The RAP was obtained from a roadway demolition site. Fig. 1 shows the coarse aggregates used in this study. All coarse aggregates used in this investigation has a maximum size of 20 mm and were sieved to get aggregates to size gradation between sieve number 20 and sieve number 4. Sieve analysis was made according to ACI committee E-701 code [17, 18] and results are illustrated in Fig. 2.
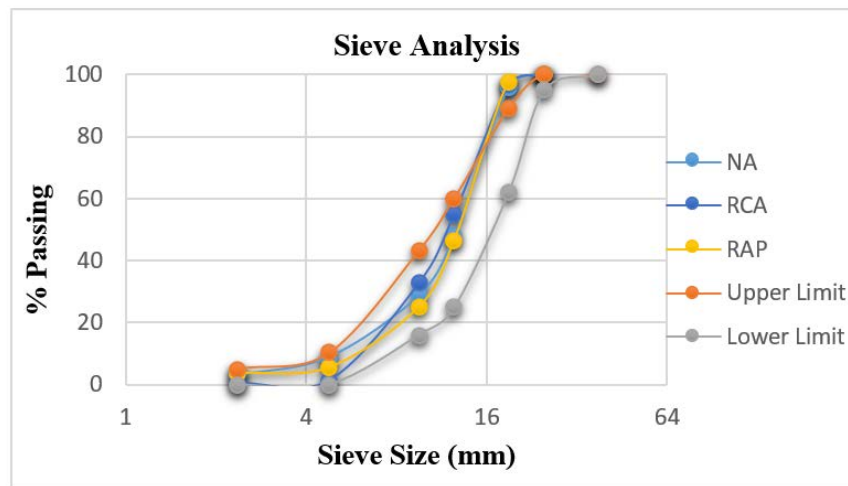

a) NA **b) RCA** **c) RAP**

Figure 1. Photos of coarse aggregate used (a) NA; (b) RCA; (c) RAP.

Figure 2. Coarse aggregates sieve analysis.

2.1.3. Light-gauge steel

Light – gauge steel or what is known as cold formed steel was used in this study with two different thicknesses (2 and 2.4 mm). This type of steel is formed or shaped at room temperature without any exposure to heat. Steel sheets are coated with zinc, which is known as galvanized steel, the main objective of this layer is to protect the steel from corrosion.

2.2. Experimental Program

2.2.1. Aggregates properties

Specific gravity and absorption tests were performed according to ASTM C 127 [19]. Results are shown in Table 1. It is observed that RCA has higher absorption value than NA, this might be attributed to the presence of cement paste in the aggregates which increases the absorption and lowers the specific gravity. Also, RAP have a lower specific gravity and a higher absorption, not as high as RCA, this is because the asphalt binder that coats RAP prevents the aggregates from absorbing too much water.

Table 1. Properties of coarse aggregates.

Property	NA	RCA	RAP
Specific Gravity (Apparent)	2.71	2.65	2.32
Specific Gravity (Bulk Dry)	2.63	2.24	2.00
Specific Gravity (Bulk SSD)	2.66	2.40	2.25
Water Absorption %	1.23	6.92	2.42
Bulk Density (Unit Weight kg/m³)	1669	1371	1316

2.2.2. Tensile test results

Yield strength, tensile strength and elongation tests were made according to ASTM A370 [20] standards for two steel samples from each thickness and the results are shown in Table 2.

Table 2. Properties of steel

Sample		Yield Strength (MPa)	Tensile Strength (MPa)	Elongation (%)
t = 2 mm	1	285	350	14.9
	2	275	350	14.9
t = 2.4 mm	3	270	357.2	12.9
	4	290	353.4	12.9

2.2.3. Concrete mix proportions

Fifteen concrete mixes were made with effective water-to-cement (w/c) ratio of 0.48 to achieve a target compressive strength of 30 MPA at 28 days. NA was replaced by RCA and RAP. Table 3 shows the mix proportions and concrete properties.

2.2.4. Concrete compressive strength

The compressive strength was determined by testing 6 cubes of 150 mm side length. Cubes were filled in three layers; each layer was stroke 35 times. Two cubes from each concrete batch were tested at 7 days, and all remaining cubes were tested at 28 days. It can be noticed that RAP-NA cubes gained more compressive strength at 7 days than RCA-NA cubes. The highest compressive strength was recorded for the 100 % NA mix followed by the combination of RCA-NA then the combination of RAP-NA, where the compressive strength decreased with the increase of RA levels. RCA-RAP compressive strength was noticed to be in between RCA-NA and RAP-NA combinations, where the compressive strength increased with the increase of RCA level except for 40 %RCA+60 %RAP and 60 %RCA+40 %RAP. This could be due to the water absorption amount.

The maximum compressive strength of 100 %NA at 28 days was 37.6 MPa. For RCA-NA combinations, the highest compressive strength was recorded for 20 %RCA+80 %NA with a value of 32.4 MPa while the lowest was recorded for 100 %RCA with a value of 20.8 MPa. For RAP-NA combinations, the highest compressive strength was recorded for 20 %RAP+80 %NA with a value of 28.0 MPa while the lowest was recorded for 100 %RAP with a value of 23.0 MPa. For RCA-RAP combinations, the highest compressive strength was recorded for 80 %RCA+20 %RAP with a value of 27.7 MPa while the lowest was recorded for 20 %RCA+80 %RAP with a value of 23.2 MPa.

Table 3. Mix proportions and concrete properties.

Mix Number	Cement (kg/m^3)	Water (kg/m^3)	Coarse Aggregate (kg/m^3)			Fine Aggregate (kg/m^3)	f_{cu} at 7 days (MPa)	f_{cu} at 28 days (MPa)
			NA	RCA	RAP			
Control Mix	375	180	1145	0	0	638	23.4	37.6
20% RCA + 80% NA	375	180	916	229	0	638	19.8	32.4
40% RCA + 60% NA	375	180	687	458	0	638	16.1	29.0
60% RCA + 40% NA	375	180	458	687	0	638	17.0	30.1
80% RCA + 20% NA	375	180	229	916	0	638	17.8	27.9
100% RCA	375	180	0	1145	0	638	13.4	20.8
20% RAP + 80% NA	375	180	916	0	229	638	20.5	28.0
40% RAP + 60% NA	375	180	687	0	458	638	16.9	26.9
60% RAP + 40% NA	375	180	458	0	687	638	19.7	27.0
80% RAP + 20% NA	375	180	229	0	916	638	16.4	25.1
100% RAP	375	180	0	0	1145	638	18.0	23.0
20% RCA + 80% RAP	375	180	0	229	916	638	17.8	23.2
40% RCA + 60% RAP	375	180	0	458	687	638	15.3	21.8
60% RCA + 40% RAP	375	180	0	687	458	638	17.7	21.9
80% RCA + 20% RAP	375	180	0	916	229	638	18.1	27.7

2.2.5. Specimens details

The flexural behavior was investigated by casting one composite beam from each steel thickness in addition to one plain concrete beam from each concrete mix. Moreover, two bare steel beams were tested as well. All beams have a square cross-section of 100×100 mm and 1200 mm length (Fig. 3b). The steel tube was made by welding two steel sheets (Fig. 3a) using an Exx70 weld type with 3 mm weld thickness. In order to avoid any slipping between concrete and steel, rivets were used on both the top and bottom surfaces of composite beams spaced at 100 mm (Fig. 3c).

a) Steel sheet detailing

b) Composite cross section


c) Longitudinal section
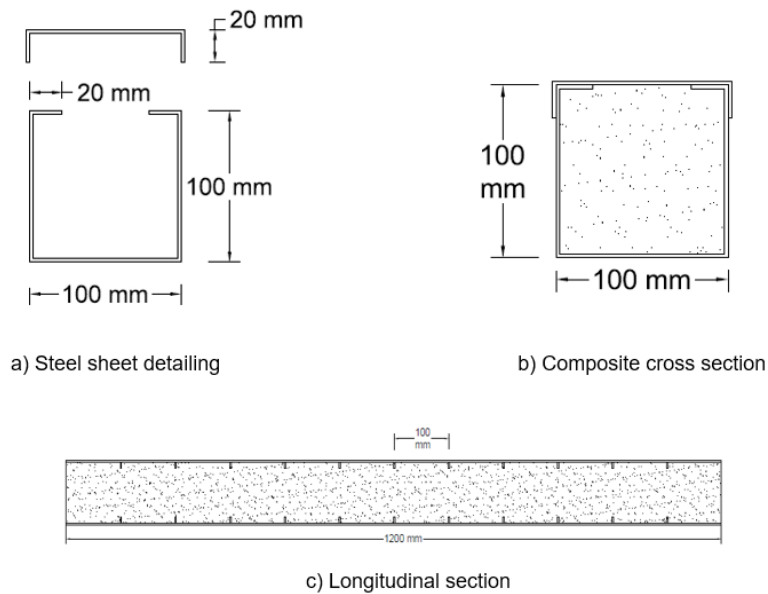
Figure 3. Composite beams sections.

For composite beams all specimens' labels start with B followed by the steel thickness then the aggregates used (R designated for RCA, P for RAP, and N for NA). For example, specimen B2.4–R20–N80 means it is a composite beam with 2.4 mm steel thickness filled with concrete containing 20 % RCA and 80 % NA. For plain concrete beams, the same labels are used without the steel thickness. Bare steel labels are B2 and B2.4 correspond to hollow steel beams with 2- and 2.4-mm thickness, respectively.

2.2.6. Test setup

Two-point loading test was conducted using a 700 kN capacity MFL Prüf-systeme Universal Testing Machine. Specimens were treated as simply supported beams lying on two concrete supports that contains two steel rods located at 100 mm from each end of the beam. Three LVDT devices with 0.01 mm accuracy were placed under the mid-span and applying load locations to measure the deflections during the test. Fig. 4 shows the test setup.
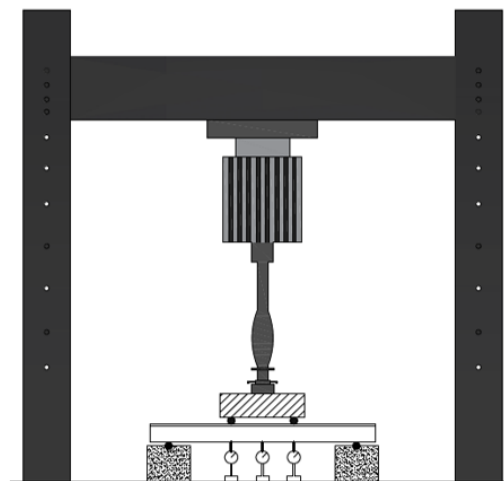

Figure 4. Test setup.

2.3. Finite Element Model

2.3.1. Parts

Composite beam is constructed from two main parts, the steel sheet cover and the concrete filling. To simulate the actual test setup, discrete rigid rods were created.

2.3.2. Materials definition

Steel was defined as an elastic plastic material with 0.3 Poisson's ratio. While concrete was defined as an elastic material, but the plasticity of concrete was defined using concrete damage plasticity. Tsai's equations were used to obtain the compressive and tensile stress-strain diagrams [21]. Fig. 5 shows the stress-strain diagrams for 100 %NA mix.
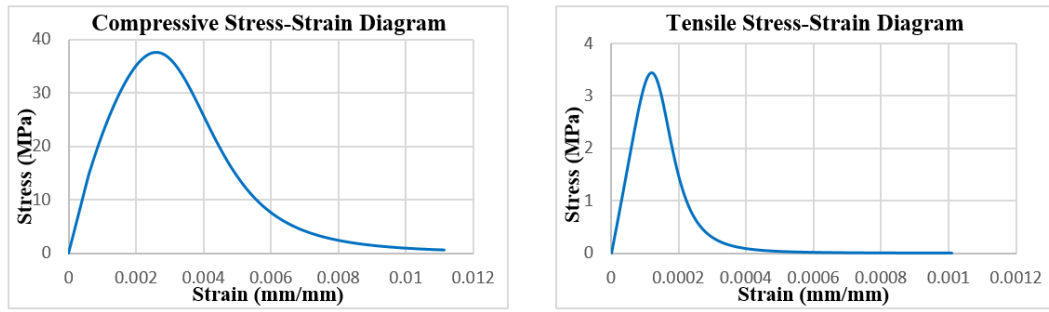
a) Compressive stress-strain diagram for 100%NA   **b) Tensile stress-strain diagram for 100%NA**
Figure 5. Compressive and tensile stress-strain diagrams for 100%NA.

2.3.3. Sections

Sections were defined as solid homogeneous type, with each section assigned to one of the pre-defined materials. Then all parts were assigned to their corresponding sections. However, test setup parts were not assigned to any section because they were defined as a discrete rigid type.

2.3.4. Meshing

Steel plate and concrete filling parts were meshed with approximate global seeds size of 30 mm and assigned to 3D stress family, while the rods were meshed with approximate global seeds size of 4.2 mm with discrete rigid element family. All parts were assigned to hexahedral element shape and meshed before the assembly of the model. Fig. 6 shows the meshed model in ABAQUS.
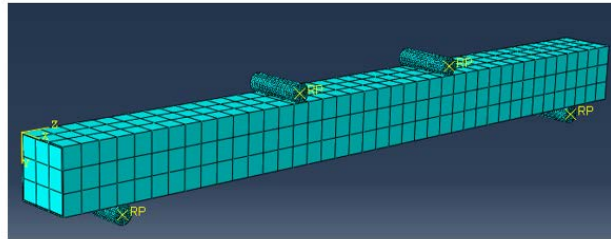

Figure 6. Model mesh.

2.3.5. Interactions

In order to ensure that all parts behave as one unit during the run, interactions must be created. General contact interaction was defined with 0.3 friction coefficient and hard contact property to ensure the hard contact between the rods and the beam, while a cohesive interface was defined between the concrete outer surface and steel inner surface.

2.3.6. Boundary conditions

Supports are defined as two rods located at 100 mm from each end of the beam, the two supports were assigned as pin supports to simulate the actual test setup. Because the rods were defined as discrete rigid elements, boundary conditions need to be assigned to their reference points. In order to be consistent with the supports, both rods were prohibited from moving in any direction. The remaining two rods were used to induce the displacement to the beam; thus, the two rods were allowed to move in the Y – direction (U2) only. A dynamic explicit step was defined to induce the displacement to the beam. This test is applicable as long as the kinetic energy is maintained to a very small quantity, and this is achieved by increasing the step time. The experimentally conducted deflection was applied to the rods using the boundary conditions (Fig. 7) with a smooth step amplitude.
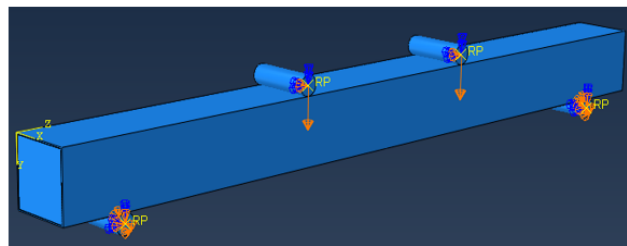
**Figure 7. Boundary conditions.**

2.3.7. History output request

The reaction forces and the mid-span deflection were requested as output data. After analysis, the load-deflection behavior obtained from ABAQUS was compared to the experimental results.

El-Nimri, R., Abdel-Jaber, M.S., Hunaiti, Y.M., Abdel-Jaber, M.

2.4. Analytical Considerations

2.4.1. Ultimate moment of resistance according to EC4 ($M_{pl,Rd}$)

The ultimate moment of resistance according to EC4 [22] is calculated based on a full plastic stress distribution on the composite cross section assuming compatibility between concrete and steel (Fig. 8).
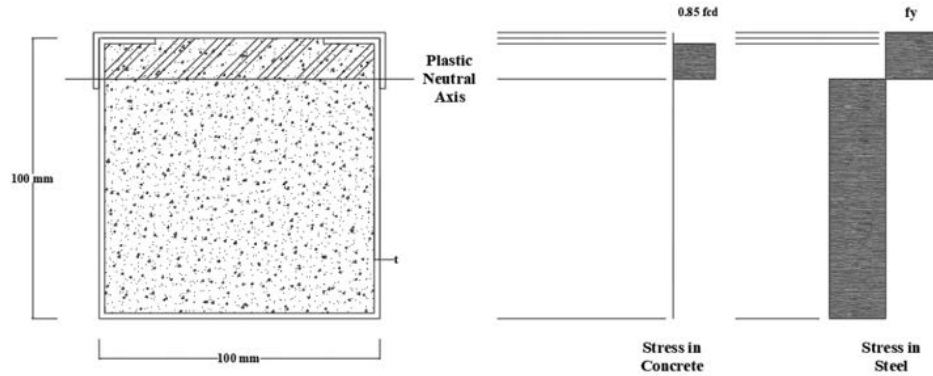

Figure 8. Stress distribution in concrete-filled steel section based on EC4.

The concrete at the tension zone is ignored, while the concrete at the compression zone is under a uniform compression stress equals to $0.85 f_{cd}$, where f_{cd} is the compressive cylinder strength of concrete at 28 days. Structural steel is stressed to its design yield strength f_{yd} in tension and compression zones.

2.4.2. Ultimate moment of resistance according to AISC-LRFD and AIJ provisions

The AISC-LRFD [23] and the AIJ [24] provisions assume that the moment capacity of HSS beams filled with concrete depends only on the steel section alone (M_{p-AISC}). Thus, the ultimate moment of resistance is assumed to be calculated based on a full plastic stress distribution on the steel section without any contribution from concrete (Fig. 9).

Bare Steel Cross Section
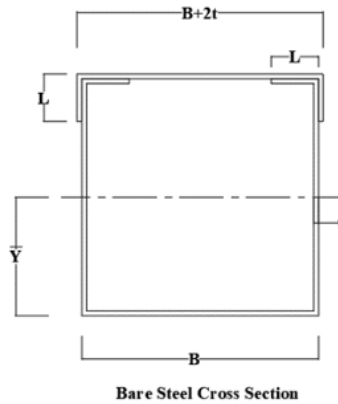
Figure 9. Bare steel cross section.

The centroid of the steel section from the bottom face of the beam (Fig. 9) is calculated using the following equation:

$$\overline{Y} = \frac{\sum A \times \overline{y}}{\sum A} \quad \text{..} \quad (1)$$

The plastic moment (M_p) is determined according to the following equation:

$$M_p = f_y \times Z \quad \text{..} \quad (2)$$

where: f_y is the steel yield stress.

Z is the section modulus (first moment of area around the centroid)

2.4.3. Ultimate moment of resistance according to RPT

Rigid plastic analysis theory is used to develop the equations of moment capacity for composite HSS beams filled with concrete [25, 26]. The flexural capacity is determined by considering the distribution of forces on both steel and concrete sections individually and introducing a bond force that represents the interaction

El-Nimri, R., Abdel-Jaber, M.S., Hunaiti, Y.M., Abdel-Jaber, M.

of concrete and steel together. The distribution of strains for full interaction and partial interaction and forces in concrete and steel across the section is shown in Fig. 10.

a) Cross section, full interaction strain and partial interaction strain

b) Forces in concrete

c) Forces in steel
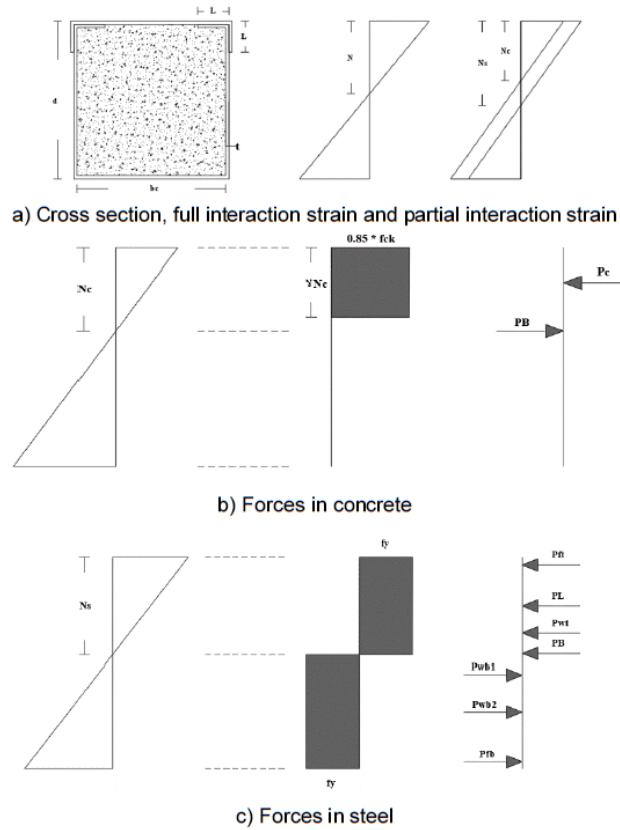
Figure 10. Rigid plastic analysis theory charts.

For the case where the neutral axis is at the overlap between the upper cap and the vertical web of the steel:

Let P_c is the force in concrete, P_B is the bond force, P_{ft} is the force in the top flange, P_L is the force in the horizontal lip, P_{wt} is the force in the vertical lip due to compression, P_{wb1} is the force in the vertical lip due to tension, P_{wb2} is the force in the web due to tension, P_{fb} is the force in the bottom flange, L is the lip length, d is the section depth, t is the steel sheets thickness, b_c is the width of concrete, f_{ck} is the characteristics compressive strength of concrete, N_c and N_s are the depth of concrete and steel neutral axes from the beam's top fiber and N is the depth of the neutral axis of the composite section from the beam's top fiber when full interaction takes place.

Considering the equilibrium of forces in concrete, the depth of the neutral axis will be given by the equation:

$$N_c = \frac{P_B + 1.7\gamma \times f_{ck} \times t \times (L-t)}{0.85\gamma \times f_{ck} \times b_c} \quad \text{...........................} \quad (3)$$

where γ is a reduction factor:

$$\gamma = 0.85 - 0.007\left(f_{ck} - 28\right) \text{...} (4)$$

Considering the equilibrium of forces in steel, the depth of the neutral axis will be given by the equation:

$$N_s = \frac{2t^2 \times f_y + 2d \times t \times f_y - P_B}{8t \times f_y} \quad \text{...........................} \quad (5)$$

Taking the moment of all forces around the top fiber of the beam, the ultimate moment capacity can be determined from the expression (6):

$$M_u = t \times f_y\left(d^2 + d \times b_c + L^2 - 4N_s^2\right) - t^2 \times f_y \times \left(b_c - 3L\right) + 3t^3 \times f_y - 0.425 f_{ck} \times \left(b_c \times t^2 + 2t^3 - 2L \times t^2 + b_c\left(\gamma \times N_c - t\right)^2\right) (6)$$

For full interaction between steel and concrete $N_s = N_c = N$, thus, the bonding force will be calculated from the expression:

$$P_B = \frac{1.7\gamma \times f_{ck} \times t \times f_y \left(b_c \times t + b_c \times d - 8L \times t + 8t^2 \right)}{8t \times f_y + 0.85\gamma \times f_{ck} \times b_c} \quad \text{........} \quad \text{..................} \quad (7)$$

For the case where the neutral axis is under the overlap between the upper cap and the vertical web of the steel:

Considering the equilibrium of forces in concrete and steel, the depth of the neutral axes will be given by the equations:

$$N_c = \frac{P_B + 1.7\gamma \times f_{ck} \times t \times (L - t)}{0.85\gamma \times f_{ck} \times b_c} \quad \text{........................} \quad (8)$$

$$N_s = \frac{2t^2 \times f_y + 2d \times t \times f_y - 4L \times t \times f_y - P_B}{4t \times f_y} \quad \text{..................} \quad (9)$$

Taking the moment of all forces around the top fiber of the beam, the ultimate moment capacity can be determined from the expression (10):

$$M_u = t \times f_y \left(d^2 + d \times b_c - L^2 - 2N_s^2 \right) + t^2 \times f_y \times (L - b_c) - 5t^3 \times f_y - 0.425 f_{ck} \times \left(b_c \times t^2 + 2t^3 - 2L \times t^2 + b_c (\gamma \times N_c - t)^2 \right) (10)$$

For full interaction between steel and concrete $N_s = N_c = N$, thus, the bonding force will be calculated from the expression:

$$P_B = \frac{1.7\gamma \times f_{ck} \times t \times f_y \left(b_c \times t + b_c \times d - 2b_c \times L + 4t^2 \right)}{4t \times f_y + 0.85\gamma \times f_{ck} \times b_c} \quad \text{...................} \quad (11)$$

3. Results and Discussion

3.1. General Behavior and Failure Modes

All composite beams failed in a ductile manner and have a flexural behavior similar to beams made with 100 % NA. Failure of the steel tube involved several local buckles that were symmetric and distributed equally at the compression zone without any tensile fracture observed at the tension zone. Beams were cut longitudinally to visualize the concrete core failure. Concrete was crushed at the compression region where local buckles took place, in addition to tensile cracks that were found at the tension zone. All the experimental observations of this study match the results obtained by Yang and Han [16]. For bare steel beams, local buckles occurred in a wider range at the compression zone, in addition to buckling of steel at the tension zone near the support region. Plain concrete beams failed in a pure flexural way, where a flexural crack initiated near the extreme tensile fiber of the beam and propagated vertically until it reached the extreme compressive fiber. Fig. 11 and 12 show the failure modes of all beams.
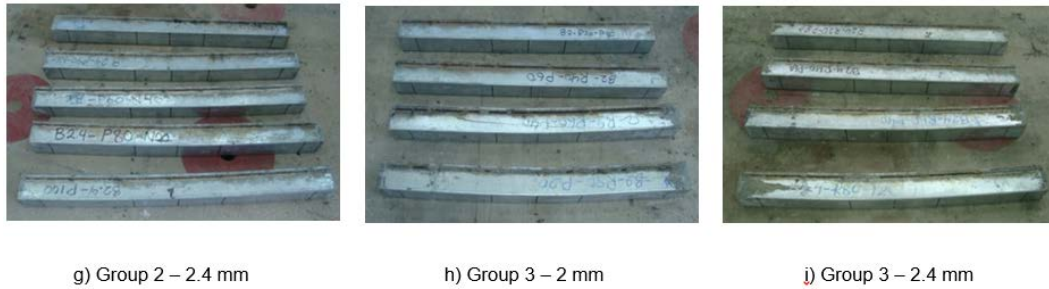

a) Control specimens   b) Bare steel beams   c) Concrete core failure

d) Group 1 – 2 mm   e) Group 1 – 2.4 mm   f) Group 2 – 2 mm

El-Nimri, R., Abdel-Jaber, M.S., Hunaiti, Y.M., Abdel-Jaber, M.

g) Group 2 – 2.4 mm   h) Group 3 – 2 mm   i) Group 3 – 2.4 mm

Figure 11. Composite beams failure modes.

Figure 12. Plain concrete beams failure modes.

3.2. Flexural Capacity

Flexural capacity of all beams is shown in Table 4. All composite beams made with 2.4 mm steel thickness had higher load capacities compared with the 2 mm steel thickness beams made from the same concrete mixes. In addition, beams within the same group developed a similar capacity pattern for both steel thicknesses (Fig. 13).

Table 4. Beams flexural capacity.

Group	Mix Number	2 mm		2.4 mm		Plain Concrete Beams (kN.m)	f_{cu} at 28 days (MPa)
		Capacity (kN)	Moment (kN.m)	Capacity (kN)	Moment (kN.m)		
Control	Control Mix	86.89	14.48	102.60	17.10	0.48	37.6
Group 1	20% RCA + 80% NA	73.08	12.18	97.32	16.22	0.71	32.4
	40% RCA + 60% NA	70.47	11.75	96.48	16.08	0.50	29.0
	60% RCA + 40% NA	69.47	11.58	90.31	15.05	0.60	30.1
	80% RCA + 20% NA	70.48	11.75	87.58	14.60	0.61	27.9
	100% RCA	65.87	10.98	87.98	14.66	0.58	20.8
Group 2	20% RAP + 80% NA	67.78	11.30	91.29	15.21	0.50	28.0
	40% RAP + 60% NA	65.47	10.91	88.58	14.76	0.57	26.9
	60% RAP + 40% NA	65.57	10.93	88.08	14.68	0.63	27.0
	80% RAP + 20% NA			84.28	14.05	0.58	25.1
	100% RAP			81.57	13.60	0.53	23.0
Group 3	20% RCA + 80% RAP	70.17	11.69	84.97	14.16	0.61	23.2
	40% RCA + 60% RAP	73.67	12.28	86.78	14.46	0.60	21.8
	60% RCA + 40% RAP	73.67	12.28	85.58	14.26	0.56	21.9
	80% RCA + 20% RAP	75.57	12.60	87.48	14.58	0.55	27.7
	Bare Steel	45.56	7.59	67.07	11.18		

Comparing the results of RACFST to the control specimens, it was observed that beams made with 100 % NA had the highest capacity among all specimens. This is attributed to the compressive strength of the concrete mixes which decreases with the use of RA. Although the compressive strength of some mixes was

lower than expected because of the water absorption amount (100 % RCA, 40% RCA+60 % RAP and 60 % RCA+40 % RAP), the behavior and capacity of RACFST were not affected. In addition, the results of B2-P80-N20 and B2-P100 did not match the capacity pattern so the results were eliminated.
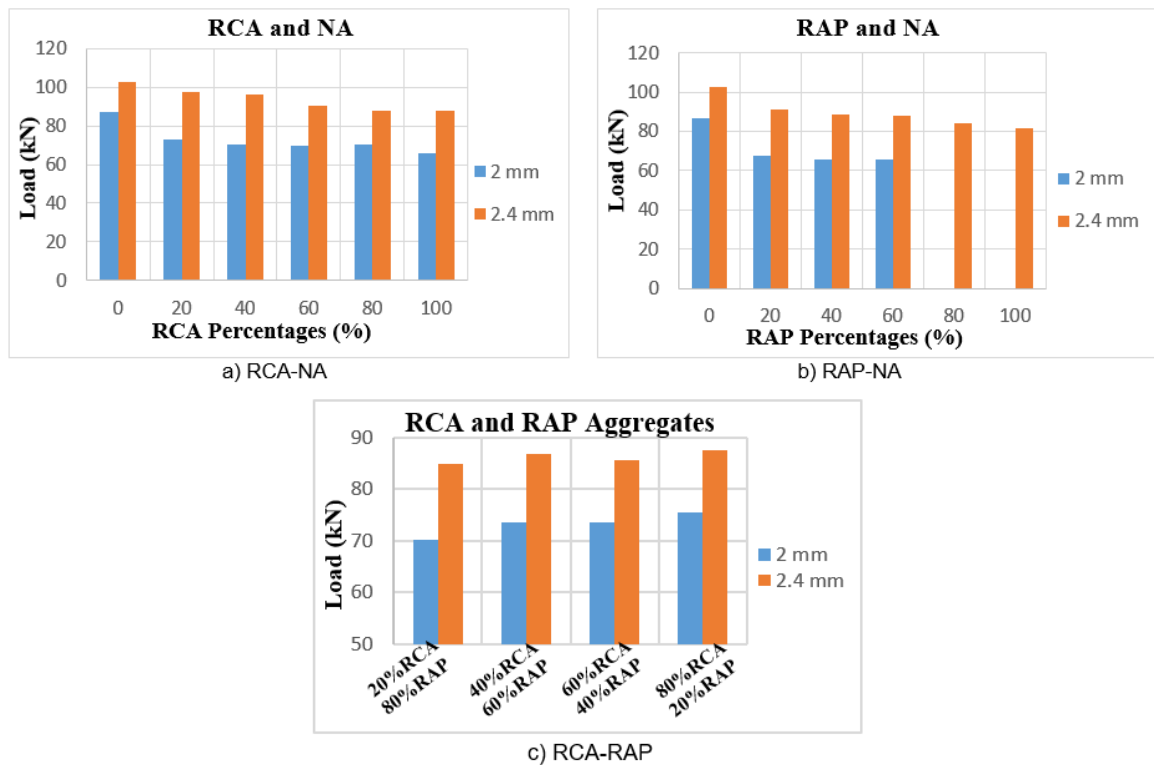

a) RCA-NA

b) RAP-NA

c) RCA-RAP

Figure 13. Beams capacity for different steel thicknesses.

The combination of RCA and NA (Group 1) gave higher load values than the combination of RAP and NA (Group 2) at the same replacement percentages, thus, RCA had the ability to sustain more loads than RAP. This is reflected on the results of the beams made with a combination of RCA and RAP (Group 3) as the capacity of beams increased with the increase of RCA percentage in the concrete mix. As opposed to their use in mixtures containing any RA (RCA and RAP) with NA where the capacity decreased with the increase of RA percentage.

Concrete filling of both NA concrete and RAC enhanced the behavior and the capacity of bare steel beams of both thicknesses. Fig. 14 shows the capacity of composite and bare steel beams.

RA had a significant influence on the flexural behavior of plain concrete beams. All beams made with RA of both RCA and RAP in all their combinations gave higher results than the plain concrete beam made with 100 %NA. The capacity of plain concrete beams containing RCA decreased with the increase of RCA percentages in the mix, while the capacity of the plain concrete beams made with RAP increased with the increase of RAP percentages except for B-P80-N20 and B-P100, this could be due to some errors in the test. For samples containing RCA and RAP, the capacity decreased with the increase of RCA percentages. Fig. 15 shows the results of the plain concrete beams.
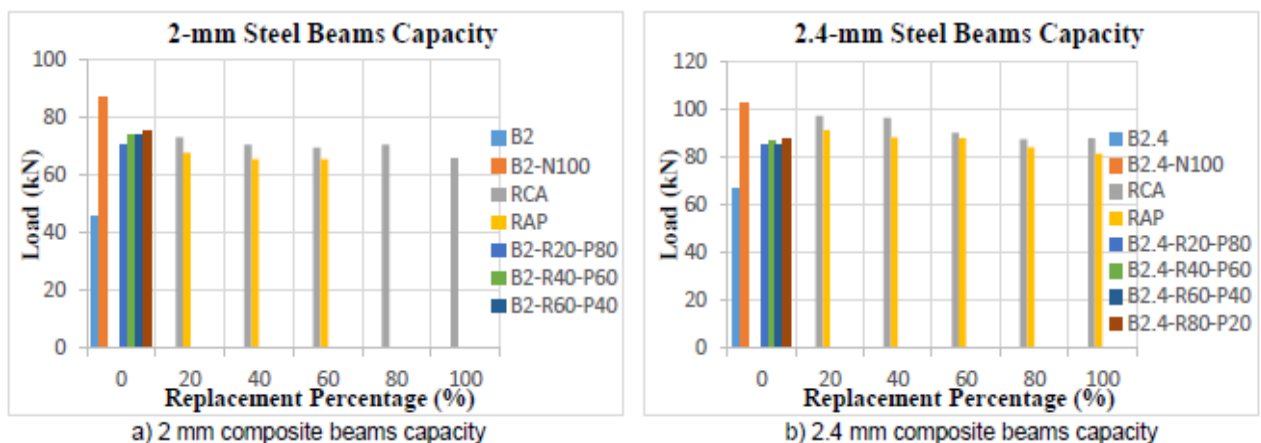

a) 2 mm composite beams capacity

b) 2.4 mm composite beams capacity

Figure 14. Capacity of composite and bare steel beams.

El-Nimri, R., Abdel-Jaber, M.S., Hunaiti, Y.M., Abdel-Jaber, M.
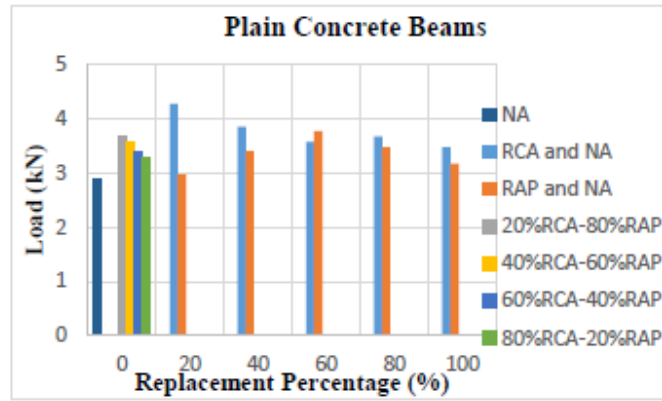
Figure 15. Capacity of the plain concrete beams.

3.3. Moment Deflection Behavior

All specimens showed an identical moment-deflection behavior, this behavior is divided into two phases. Phase one starts from the zero moments up to about 60 % of the ultimate moment capacity where the beams had a linear behavior which indicates the elastic performance of the specimens.

After this point, higher deflection values were measured with a slight increase in load, this represents phase two that indicates the ductile response of the beam specimens with gradually decreasing stiffness. Fig. 16 shows the moment deflection behavior of composite and bare steel beams.
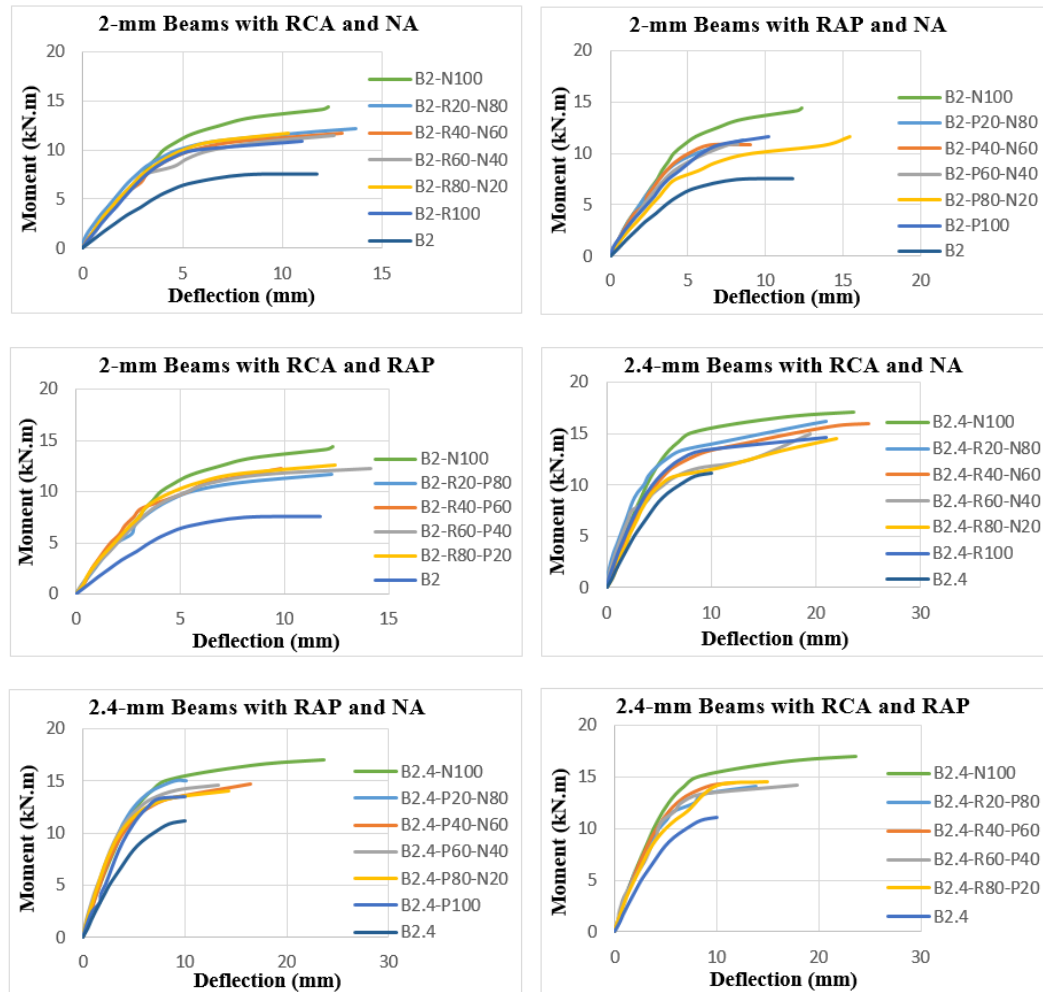
Figure 16. Moment deflection behavior.

The deflected shape of all beams was the same and had the shape of approximately a half sine wave. Yang and Han [16] reported similar observation. Specimens B2-R40-N60 and B2.4-R80-P20 were selected to illustrate the development of the deflected shape of the composite beams (Fig. 17), where the deflection values were plotted at different moment levels for each sample.
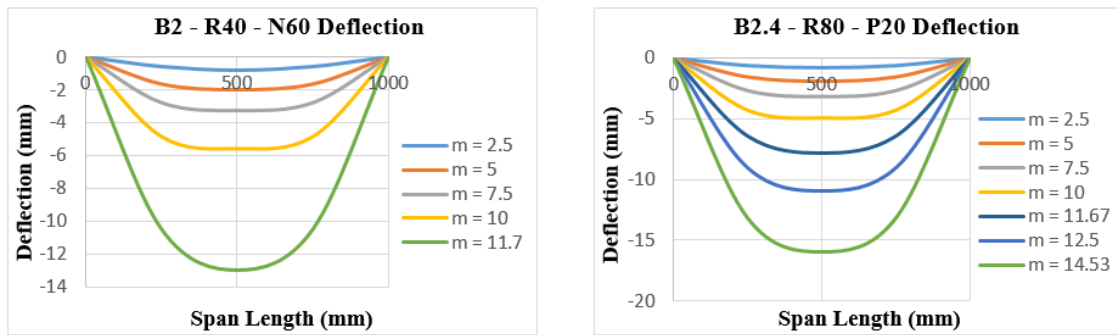
Figure 17. Deflection development at different moment levels.

3.4. Theoretical Ultimate Moment of Resistance

In order to investigate the validity of codes' equations, the ultimate moment capacities were calculated according to EC4, AISC-LRFD, AIJ, and the RPT. Tables 5 and 6 show the theoretical predicted values compared to the experimental results. Mean, Coefficient of Variation (COV), and the reduction percent (%) were also calculated. All codes gave a safe prediction of the ultimate moment capacities of composite beams as the RPT gave the closest moment value of all codes with a COV and a reduction percent of 0.0682 and about 12 % for samples with 2 mm steel and a COV and a reduction percent of 0.0526 and almost 18 % for samples with 2.4 mm steel.

Table 5. Theoretical capacity of composite beams with 2 mm steel thickness.

Mix	M_{ue}	EC4		AISC-LRFD		AIJ		RPT	
		$M_{pl,Rd}$	$\dfrac{M_{pl,Rd}}{M_{ue}}$	$M_{u\text{-}AISC}$	$\dfrac{M_{u-AISC}}{M_{ue}}$	$M_{u\text{-}AIJ}$	$\dfrac{M_{u-AIJ}}{M_{ue}}$	$M_{u\text{-}RPT}$	$\dfrac{M_{u-RPT}}{M_{ue}}$
B2 – N100	14.48	10.28	0.710	9.66	0.667	9.66	0.667	10.49	0.725
B2 – R20 – N80	12.18	10.24	0.841	9.66	0.793	9.66	0.793	10.45	0.858
B2 – R40 – N60	11.75	10.21	0.869	9.66	0.822	9.66	0.822	10.41	0.886
B2 – R60 – N40	11.58	10.22	0.883	9.66	0.834	9.66	0.834	10.42	0.900
B2 – R80 – N20	11.75	10.20	0.868	9.66	0.822	9.66	0.822	10.40	0.885
B2 – R100	10.98	10.13	0.923	9.66	0.880	9.66	0.880	10.25	0.934
B2 – P20 – N80	11.30	10.20	0.903	9.66	0.855	9.66	0.855	10.40	0.921
B2 – P40 – N60	10.91	10.19	0.934	9.66	0.885	9.66	0.885	10.39	0.952
B2 – P60 – N40	10.93	10.19	0.932	9.66	0.884	9.66	0.884	10.39	0.951
B2 – P80 – N20									
B2 – P100									
B2 – R20 – P80	11.69	10.16	0.869	9.66	0.826	9.66	0.826	10.28	0.879
B2 – R40 – P60	12.28	10.14	0.826	9.66	0.787	9.66	0.787	10.27	0.836
B2 – R60 – P40	12.28	10.15	0.827	9.66	0.787	9.66	0.787	10.27	0.836
B2 – R80 – P20	12.60	10.20	0.810	9.66	0.767	9.66	0.767	10.40	0.826
Mean		0.861		0.816		0.816		0.876	
Coefficient of variation		0.0683		0.0699		0.0699		0.0682	
Reduction Percent (%)		13.9		18.4		18.4		12.4	

Table 6. Theoretical capacity of composite beams with 2.4 mm steel thickness.

Mix	M_{ue}	EC4		AISC-LRFD		AIJ		RPT	
		$M_{pl,Rd}$	$\dfrac{M_{pl,Rd}}{M_{ue}}$	$M_{u\text{-}AISC}$	$\dfrac{M_{u-AISC}}{M_{ue}}$	$M_{u\text{-}AIJ}$	$\dfrac{M_{u-AIJ}}{M_{ue}}$	$M_{u\text{-}RPT}$	$\dfrac{M_{u-RPT}}{M_{ue}}$
B2.4 – N100	17.10	12.22	0.715	11.58	0.677	11.58	0.677	12.45	0.728
B2.4 – R20 – N80	16.22	12.18	0.751	11.58	0.714	11.58	0.714	12.30	0.759
B2.4 – R40 – N60	16.08	12.15	0.756	11.58	0.720	11.58	0.720	12.27	0.763
B2.4 – R60 – N40	15.05	12.16	0.808	11.58	0.769	11.58	0.769	12.28	0.816
B2.4 – R80 – N20	14.60	12.14	0.832	11.58	0.793	11.58	0.793	12.25	0.839
B2.4 – R100	14.66	12.06	0.823	11.58	0.790	11.58	0.790	12.16	0.829
B2.4 – P20 – N80	15.21	12.14	0.798	11.58	0.761	11.58	0.761	12.25	0.805
B2.4 – P40 – N60	14.76	12.13	0.822	11.58	0.784	11.58	0.784	12.24	0.829
B2.4 – P60 – N40	14.68	12.13	0.826	11.58	0.789	11.58	0.789	12.24	0.834
B2.4 – P80 – N20	14.05	12.11	0.862	11.58	0.824	11.58	0.824	12.22	0.870
B2.4 – P100	13.60	12.09	0.889	11.58	0.852	11.58	0.852	12.19	0.897
B2.4 – R20 – P80	14.16	12.09	0.854	11.58	0.818	11.58	0.818	12.19	0.861
B2.4 – R40 – P60	14.46	12.07	0.835	11.58	0.801	11.58	0.801	12.17	0.842
B2.4 – R60 – P40	14.26	12.07	0.846	11.58	0.812	11.58	0.812	12.17	0.854
B2.4 – R80 – P20	14.58	12.40	0.851	11.58	0.794	11.58	0.794	12.25	0.840
Mean		0.818		0.780		0.780		0.824	
Coefficient of variation		0.0550		0.0569		0.0569		0.0526	
Reduction Percent (%)		18.2		22.0		22.0		17.6	

3.5. FEA Results

In order to ensure a static analysis using a dynamic explicit step, the kinetic energy throughout the analysis must be a very small quantity. Fig. 18 shows the kinetic energy of Sample B2 – P60 – N40.
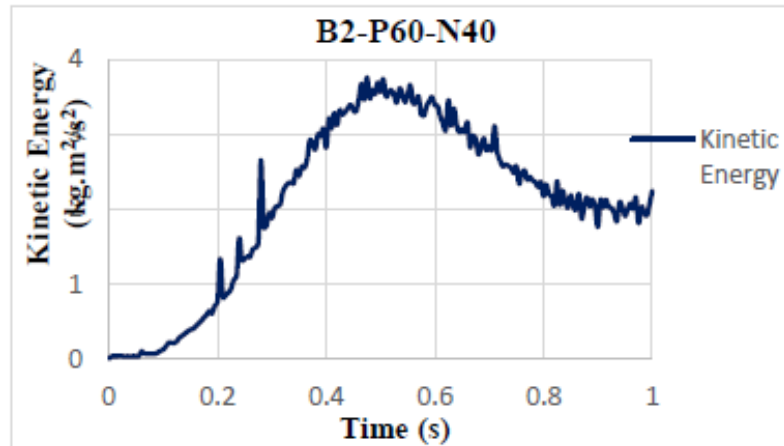
Figure 18. Kinetic energy of beam B2 – P60 – N40.

All beams analyzed in ABAQUS showed nearly the same deflected shape as the experimental one. Fig. 19 shows the deflected shape obtained from ABAQUS for the sample B2-R20-N80.

The maximum principal plastic strain results of FE simulation for the sample B2.4-N100 is presented in Fig. 20. It illustrates the cracking of concrete based on the stress–strain relationship. The results agreed well with the experimental concrete cracks that were found after cutting the composite beams.
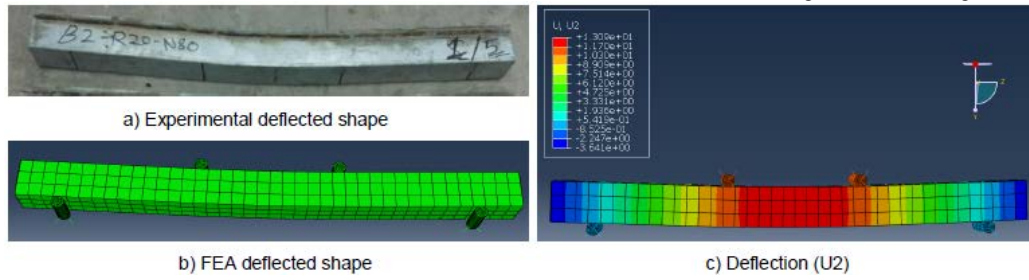
a) Experimental deflected shape

b) FEA deflected shape

c) Deflection (U2)

Figure 19. Experimental and FEA deflected shape for beam B2-R20-N80.
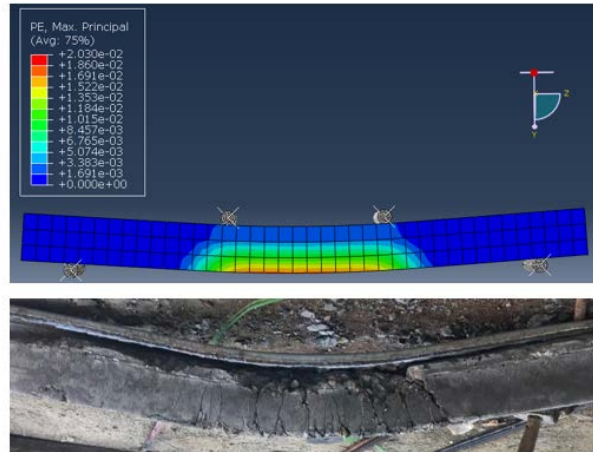

Figure 20. Maximum principal plastic strain for B2.4-N100.

Reaction forces and mid-span deflections were the history output requests for the analysis. All beams analyzed in ABAQUS showed nearly the same Load-Deflection behavior as the experimental behavior. Fig. 21 and 22 show a comparison between the experimental load deflection behavior and the one obtained from ABAQUS.
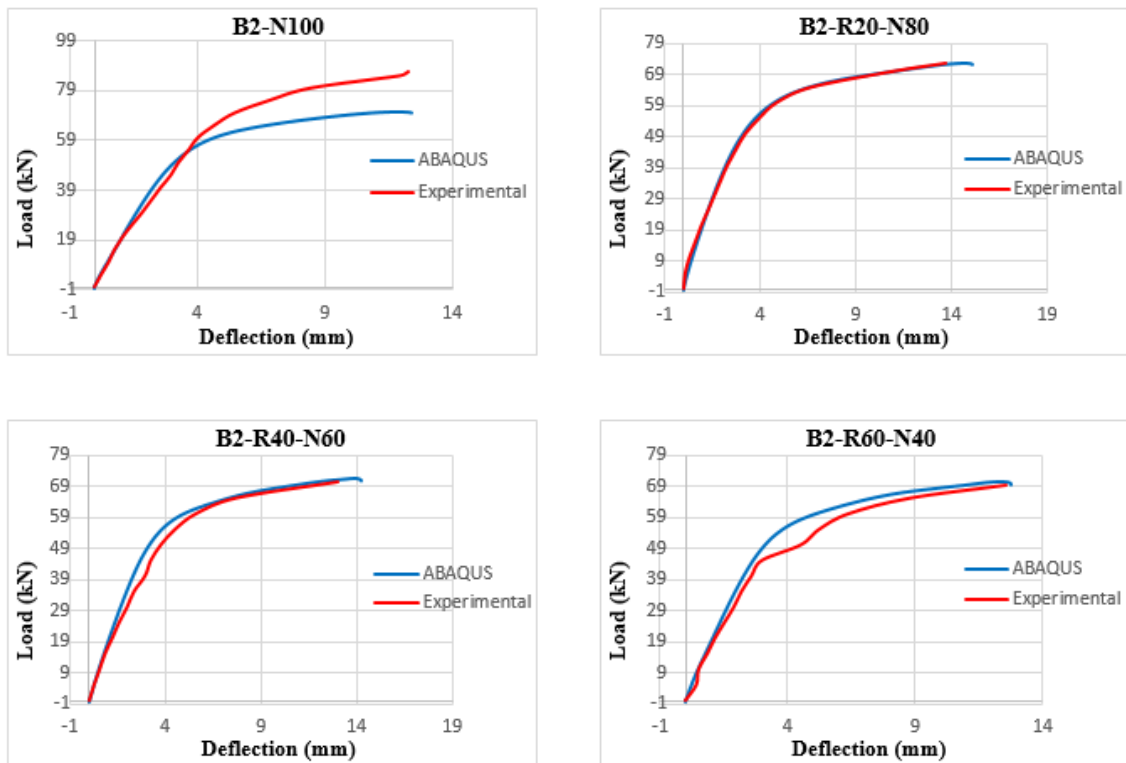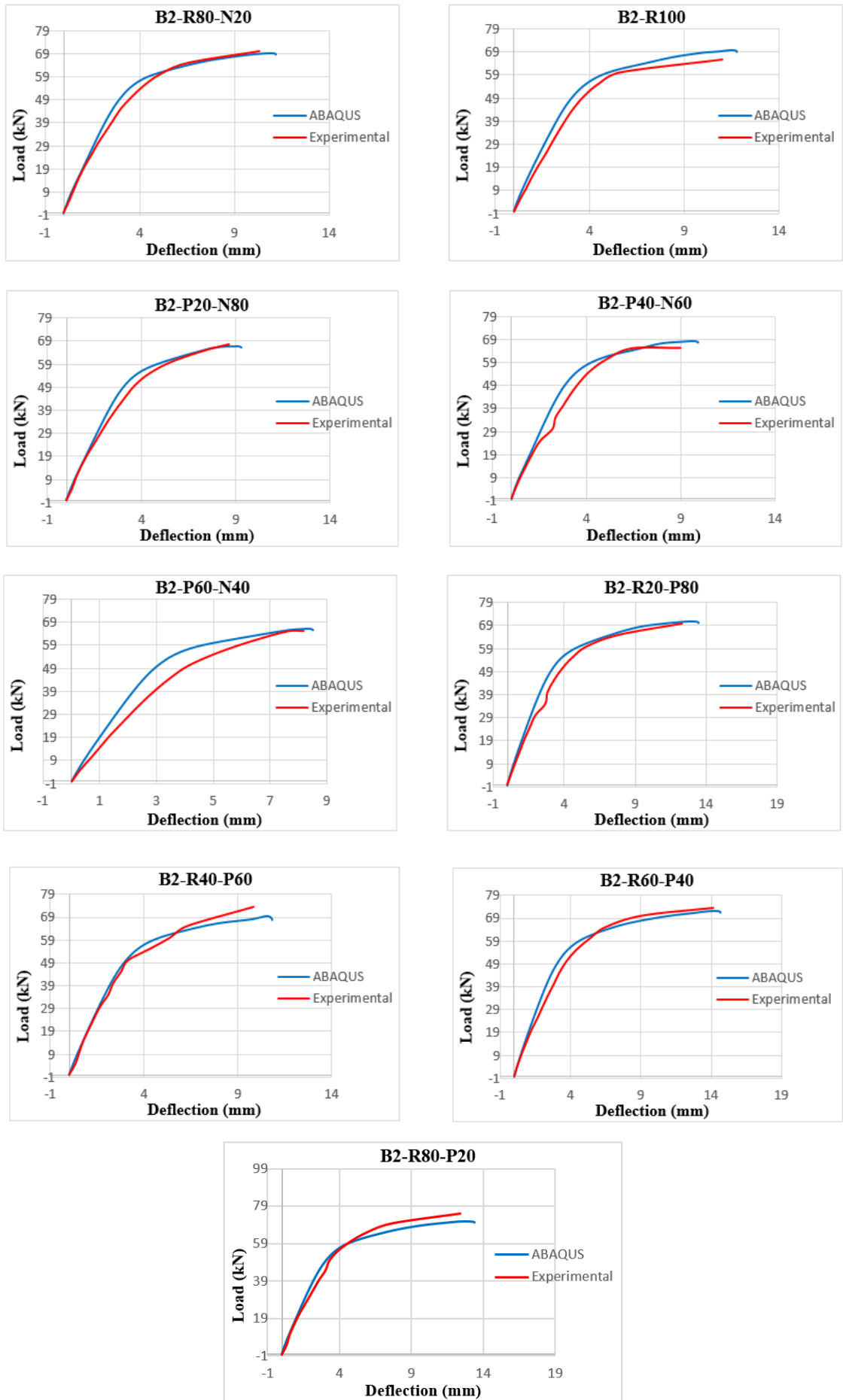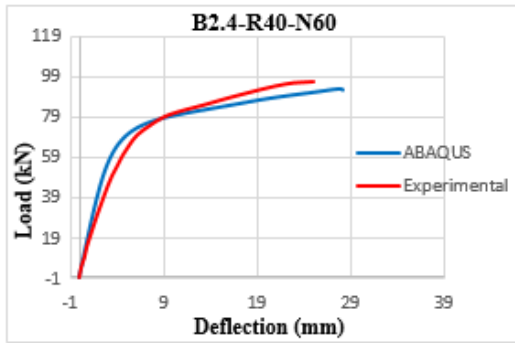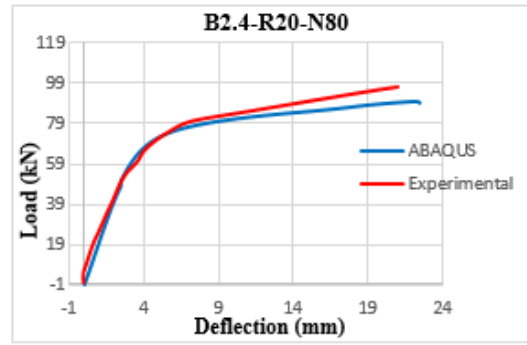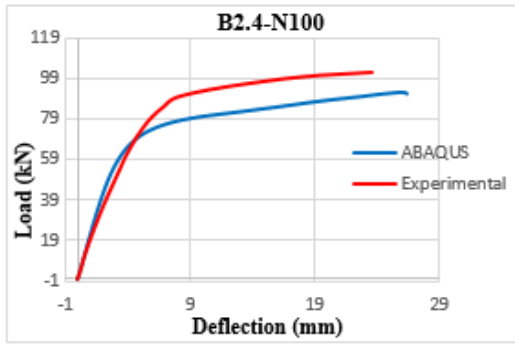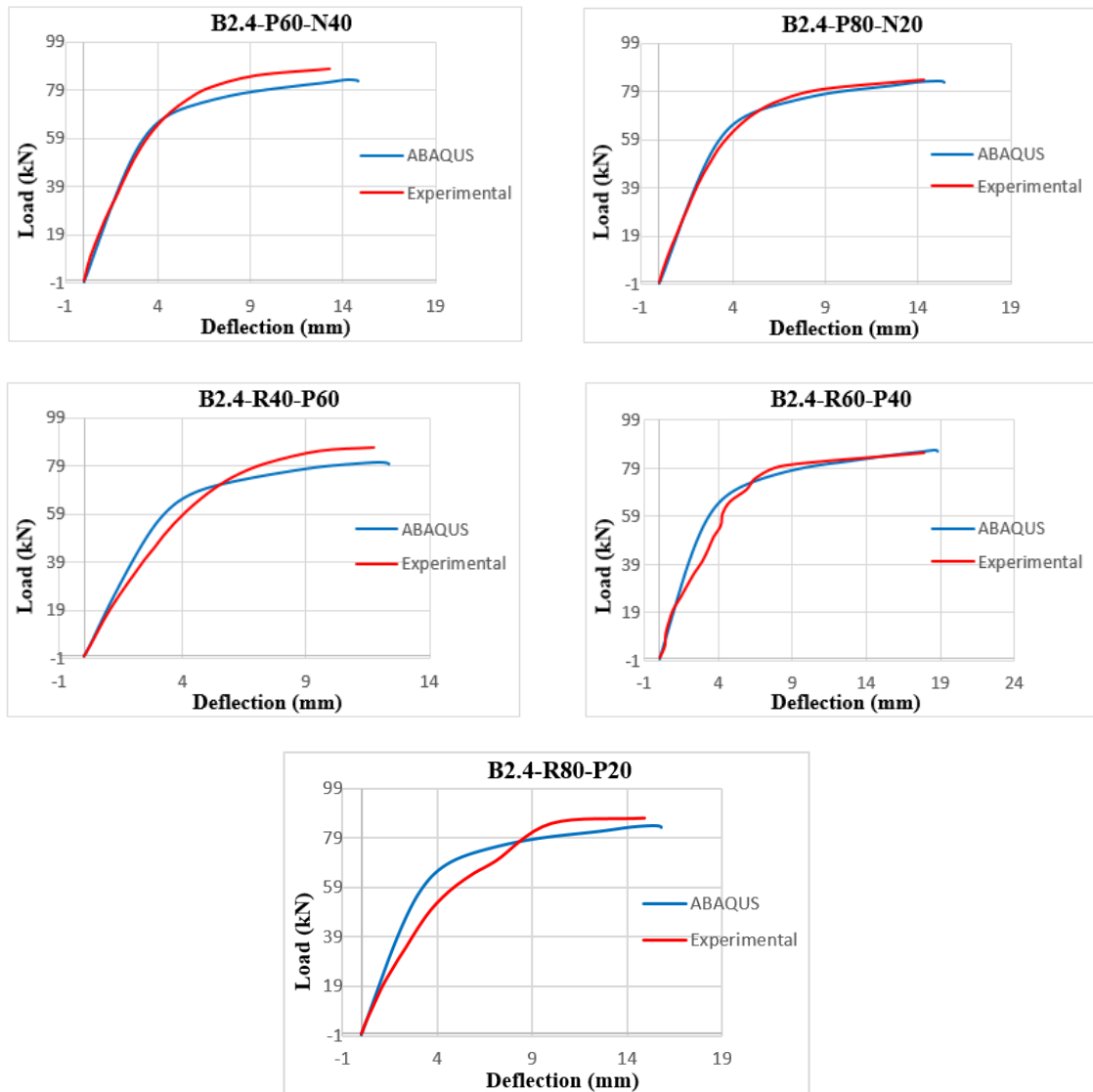
Figure 21. Comparison between experimental and ABAQUS load deflection behavior for 2 mm steel.
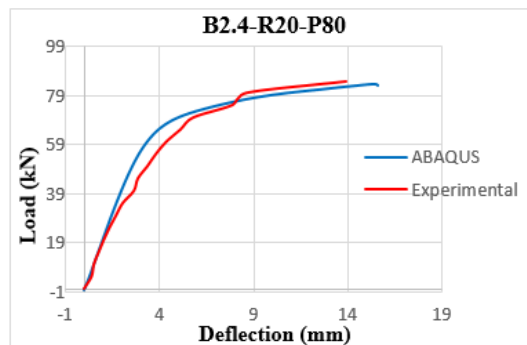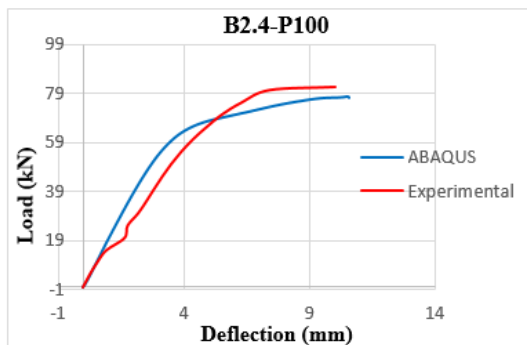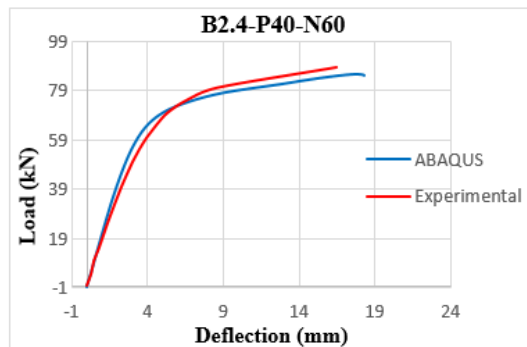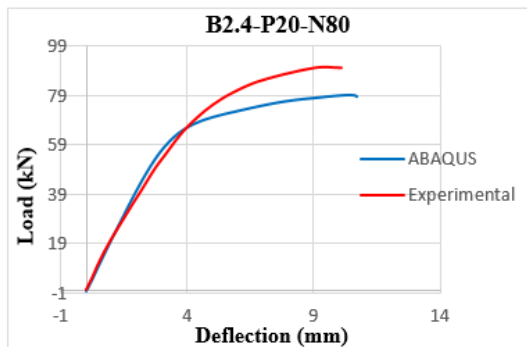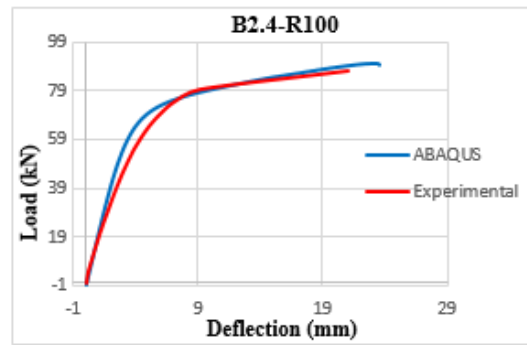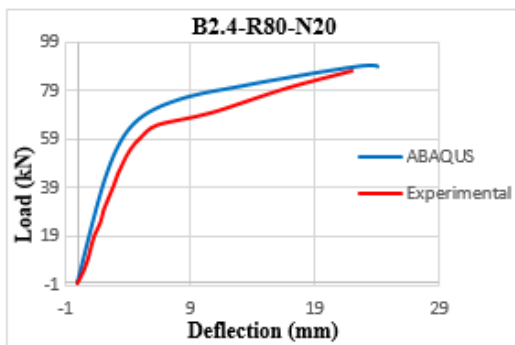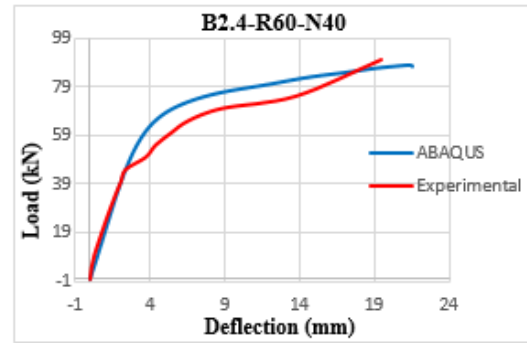
Figure 22. Comparison between experimental and ABAQUS load deflection behavior for 2.4 mm steel.

3.6. Discussion

In general, all composite columns filled with recycled concrete showed a reduction in capacity. For samples with 2 mm steel thickness, the moment capacities of the RACFST for RCA-NA, RAP-NA, and RCA-RAP were about (16 % to 24 %), (22 % to 25 %), and (13 % to 19 %) lower than the control specimen B2-N100, respectively. While for samples with 2.4 mm steel thickness, the moment capacities for RCA-NA, RAP-NA, and RCA-RAP were about (5 % to 15 %), (11 % to 21 %), and (15 % to 17 %) lower than the control specimen B2.4-N100, respectively. This reduction for RCA-NA could be attributed to the presence of old cement paste that requires higher water absorption. While for RAP-NA can be attributed to the presence of asphalt binder coating which weakens the bond between the aggregate and the concrete matrix. For RCA-RAP combination, the moment capacities were ranging between RCA-NA and RAP-NA combinations. This could be an indication that RCA-RAP could be a promising technique in replacing NA for future constructions.

Concrete filling enhanced the behavior and capacity of bare steel beams. For samples with 2 mm steel thickness, the moment capacity B2 was enhanced by about (45 % to 60 %), (44 % to 49 %), (54 % to 66 %), and 91 % for RCA-NA, RAP-NA, RCA-RAP, and the control beam B2-N100, respectively. While for samples with 2.4 mm steel thickness, the moment capacity of B2.4 was enhanced by about (31 % to 45 %), (22 % to 36 %), (27 % to 30 %), and 53 % for RCA-NA, RAP-NA, RCA-RAP, and the control beam B2.4-N100, respectively. It can be noticed that the enhancement of the moment capacity caused by the concrete filling decreases with the increase of the steel thickness used.

RA had a positive influence on the flexural behavior of all plain concrete beams. The capacity increased with the increase of RAP and decreased with the increase of RCA.

RA did not have a significant effect on the deflection behavior. RACFST developed similar moment deflection behavior as the control beams.

4. Conclusions

The flexural behavior of light-gauge steel filled with normal and recycled concrete was investigated in this study. Different coarse aggregate combinations were used: RCA-NA, RAP-NA, and RCA-RAP with different replacement levels. The following conclusions can be drawn from this study:

1. It is feasible to use RA of both types (RCA and RAP) in cold formed steel filled sections with low to medium compressive strength, as they gave promising results.

2. The flexural behavior of HSS beams filled with RAC is similar to the corresponding control samples that were filled with NA concrete at all loading stages.

3. All beams failed in a ductile manner and developed moments in excess of the theoretically predicted values. Buckling of steel sheets, cracking and separation of concrete from steel governed the failure of composite beams.

4. The ultimate capacity of RACFST decreased with the increase of the RA percentages. The optimum mixes were (20 %RCA+80 %NA), (20 %RAP+80 %NA), and (80 %RCA+20 %RAP) for RCA-NA, RAP-NA, and RCA-RAP combinations, respectively.

5. Concrete infill enhanced the capacity of HSS beams. Moreover, concrete filling provides more rigidity to hollow steel beams and enhances their ability to resist buckling as well.

6. All beams developed similar moment-deflection behavior until they reached the code predicted ultimate moments, then, exhibited a slight change in the moment-deflection behavior up to failure.

7. The RA of both types had a good influence on the flexural behavior of plain concrete beams, the capacity decreases with the increase of RCA percentages and increases with the increase of RAP percentages. The optimum mixes were reported to be (20 %RCA+8 0%NA), (60 %RAP+40 %NA), and (20 %RCA+80 %RAP) for RCA-NA, RAP-NA, and RCA-RAP combinations, respectively.

8. The loading capacities of RACFST can be conservatively predicted by the current code provisions of EC4, AISC-LRFD, AIJ, and the RPT recommendations, as the AISC-LRFD and AIJ codes significantly underestimated the moment capacity of RACFST while the RPT gives the best prediction of the test results than other methods with a COV value of 0.0682 and 0.0526 for composite beams made with 2- and 2.4-mm steel sheets, respectively.

9. Based on AISC-LRFD and AIJ code provisions, when a composite member is subjected to a pure flexural load, the predicted moment capacity depends only on the steel section, and thus it will be conservative no matter what type of aggregates is used.

10. FEA results showed reasonable agreement and high degree of similarity with the experimental results, however, there were several differences between FEA and experimental results. Numerical results proved that ABAQUS software is effective and predicts the ultimate capacity of concrete filled tubes with acceptable accuracy.

5. Acknowledgements

References

1. Corinaldesi, V. Mechanical and elastic behaviour of concretes made of recycled-concrete coarse aggregates. Constr. Build. Mater. 2010. Vol. 24. No. 9. Pp. 1616–1620.

2. Etxeberria, M., Vázquez, E., Marí, A., Barra, M. Influence of amount of recycled coarse aggregates and production process on properties of recycled aggregate concrete. Cem. Concr. Res. 2007. Vol. 37. No. 5. Pp. 735–742.

3. Rahal, K. Mechanical properties of concrete with recycled coarse aggregate. Mechanical properties of concrete with recycled coarse aggregate. 2007. Vol. 42. No. January. Pp. 407–415.

4. Shatarat, N.K., Katkhuda, H.N., Hyari, K.H., Asi, I. Effect of using recycled coarse aggregate and recycled asphalt pavement on the properties of pervious concrete. Struct. Eng. Mech. 2018. Vol. 67. No. 3. Pp. 283–290.

5. Al-Tarawneh, K.L. Flexural Performance of Reinforced Concrete Beams Made with Two Types of Coarse Recycled Aggregates. RCA AND RAP. Unpublished Master's Thesis, The University of Jordan, Amman, Jordan, 2018.

El-Nimri, R., Abdel-Jaber, M.S., Hunaiti, Y.M., Abdel-Jaber, M.

6. Katkhuda, H.I., Shatarat, N. Shear behavior of reinforced concrete beams using treated recycled concrete aggregate. Constr. Build. Mater. 2016. Vol. 125. Pp. 63–71.

7. Knaack, A.M., Kurama, Y.C. Behavior of reinforced concrete beams with recycled concrete coarse aggregates. J. Struct. Eng. (United States). 2015. Vol. 141. No. 3.

8. Shatarat, N., Alhaq, A.A., Katkhuda, H., Jaber, M.A. Investigation of axial compressive behavior of reinforced concrete columns using Recycled Coarse Aggregate and Recycled Asphalt Pavement aggregate. Constr. Build. Mater. 2019. Vol. 217. No. May. Pp. 384–393.

9. Huang, B., Shu, X., Burdette, E.G. Mechanical properties of concrete containing recycled asphalt pavements. Magazine of Concrete Research. 2006. Vol. 58. No. 5. Pp. 313–320

10. Larbi, R., Morsli, M., Bali, A., Benyoussef, E.-H. Mechanical and elastic properties of concretes made with recycled asphalt. International Journal of Advances in Mechanical and Civil Engineering. 2017. Vol. 4. No. 3.

11. Okafor, F.O. Performance of recycled asphalt pavement as coarse aggregate in concrete. Leonardo Electron. J. Pract. Technol. 2010. Vol. 9. No. 17. Pp. 47–58.

12. Hunaiti, Y.M. Strength of composite sections with foamed and lightweight aggregate concrete J. Mater. Civ. Eng. 1997. Vol. 9. No. 2. Pp. 58–61.

13. Nakamura, S.-i., Morishita, H. Bending strength of concrete-filled narrow-width steel box girder. J. Constr. Steel Res. 2008. Vol. 64. No. 1. Pp. 128–133.

14. Soundararajan, A., Shanmugasundaram, K. Flexural behaviour of concrete-filled steel hollow sections beams. J. Civ. Eng. Manag. 2008. Vol. 14. No. 2. Pp. 107–114.

15. Varma, A.H., Ricles, J.M., Sause, R., Lu, L.W. Experimental behavior of high strength square concrete-filled steel tube beam-columns. J. Struct. Eng. 2002. Vol. 128. No. 3. Pp. 309–318.

16. Yang, Y.F., Man, L.H. Compressive and flexural behaviour of recycled aggregate concrete filled steel tubes (RACFST) under short-term loadings. Steel Compos. Struct. 2006. Vol. 6. No. 3. Pp. 257–284.

17. Building Code Requirements for Structural Concrete (ACI 318-14) Commentary on Building Code Requirements for Structural Concrete (ACI 318R-14) An ACI Standard and Report from HIS. 2014.

18. Bulletin, A.C.I.E. Aggregates for Concrete ACI Education Bulletin E1-07. Concr. Constr. 2007. P. 29.

19. ASTM. ASTM C 127-08: Standard Test Method for Density, Relative Density (Specific Gravity), and Absorption of Fine Aggregate. 2008. Pp. 1–7.

20. ASTM. A370: Standard Test Methods and Definitions for Mechanical Testing of Steel Products. ASTM Int. 2014. Pp. 1–50.

21. Allouzi, R., Alkloub, A., Naghawi, H., Al-Ajarmeh, R. Fracture Modeling of Concrete in Plain and Reinforced Concrete Members. Int. J. Civ. Eng. 2019. Vol. 17. No. 7. Pp. 1029–1042.

22. Europeenne, N. EUROPEAN STANDARD Eurocode 4: Design of composite steel and concrete structures-Part 1-1: General rules and rules for buildings. 2004.

23. Load and resistance factor design specification for structural steel buildings. 1999.

24. AIJ (1997). Recommendations for design and construction of concrete filled steel tubular structures. Architectural Institute of Japan, Tokyo, Japan.

25. Valsa Ipe, T., Sharada Bai, H., Manjula Vani, K., Iqbal, M.M.Z. Flexural behavior of cold-formed steel concrete composite beams. Steel Compos. Struct. 2013. Vol. 14. No. 2. Pp. 105–120.

26. Jyothi, K.N., Valsa Ipe. T. Performance of Infilled Cold Formed Steel Channel Section Beams. Int. J. Eng. Res. 2015. Vol. V4. No. 12. Pp. 446–451.

Contacts:

Rola El-Nimri, rola.elnimri@gmail.com

Mu'tasim Abdel-Jaber, m.abduljaber@ju.edu.jo

Yasser Hunaiti, hunaiti@ju.edu.jo

Ma'en Abdel-Jaber, maen.abdel-jaber@htu.edu.jo